From a profiled diffuser to an optimized absorber

Wu, T, Cox, TJ and Lam, YW

http://dx.doi.org/10.1121/1.429596

From a profiled diffuser to an optimized absorber

T. Wu, T. J. Cox, and Y. W. Lam
School of Acoustics and Electronic Engineering, University of Salford, Salford M5 4WT, United Kingdom

(Received 28 October 1999; revised 24 March 2000; accepted 23 April 2000)

The quadratic residue diffuser was originally designed for enhanced scattering. Subsequently, however, it has been found that these diffusers can also be designed to produce exceptional absorption. This paper looks into the absorption mechanism of the one-dimensional quadratic residue diffuser. A theory for enhanced absorption is presented. Corresponding experiments have also been done to verify the theory. The usefulness of a resistive layer at the well openings has been verified. A numerical optimization was performed to obtain a better depth sequence. The results clearly show that by arranging the depths of the wells properly in one period, the absorption is considerably better than that of a quadratic residue diffuser. © *2000 Acoustical Society of America.* [S0001-4966(00)01308-4]

PACS numbers: 43.55.Ev, 43.55.Dt [JDQ]

INTRODUCTION

Profiled diffusers were invented by Schroeder[1] in the 1970s. An example of the one-dimensional Schroeder diffusers is shown in Fig. 1. They are periodic surface structures with rigid construction; the elements of the structure are wells of the same width separated by thin fins. Within one period, the depths of the elements vary according to a pseudo-stochastic sequence.

The basis behind the Schroeder diffuser is as follows: When the sound is incident on the surface of the structure, plane waves travel down and up each wells. The returning waves at the entrances of the wells no longer have the same phases because of the different depths they have traveled. If the phase differences are appropriate, the diffuser will disperse the sound rather than specularly reflect it, and thus generate diffusion in the far field. For this purpose, Schroeder exploited the Fourier transform of the surface reflection factors to choose the depth sequence in one period, as it approximately gives the far field diffracted pressure distribution. The most popular Schroeder diffuser is the quadratic residue diffuser (QRD), which employs the quadratic residue sequence to determine the well depth. The Fourier transform of the QRD surface reflection factors gives a constant power spectrum leading to even energy diffraction lobes. The QRD has been widely used in concert halls, theatres, and studio monitor rooms.[2,3]

The QRD was designed to diffuse rather than absorb sound, although for some time there was anecdotal evidence of absorption. Dramatic levels of absorption from Schroeder diffusers were measured by Fujiwara and Miyajima[4] in 1992. They reported the unexpectedly high measured absorption of a poorly constructed QRD at low frequency, which they could not explain. It was later found[5] that the quality of construction was to blame for some of the excess absorption. Kuttruff[6] tried to explain the absorption by assuming that the total sound pressure on the diffuser plane was constant. This led to an absorption based on the same average surface admittance, which generated additional possible air flow between adjacent wells. This additional air flow was associated with the excess absorption of the diffusers, but this air flow is not explicitly included in the average admittance model. He could only find agreement with Fujiwara's data when he reduced the width of the wells to an unrealistic one-tenth of the width in the real diffuser. Mechel thoroughly investigated the Schroeder diffuser in his paper in Acustica[7] and in greater detail in his book.[8] He described the absorption effect for the near field as well as the directivity for the far field analysis, with and without viscous and thermal losses in and in front of the wells using a Fourier wave decomposition model. Mechel demonstrated that resistive layers at the well entrances turn these diffuser structures into potentially useful and practical absorbers. Furthermore, he discussed how using a primitive root sequence to determine the well depths of the structure could result in a better absorber than the more common quadratic residue sequence. Unfortunately, there were no corresponding experimental results to verify the findings, something which is added later in this paper.

In this paper, the sound absorption by the one-dimensional Schroeder diffuser is studied both theoretically and experimentally. The Schroeder structure can be used to make an effective absorber or a low loss diffuser depending on the geometry and construction of the device. Since absorption is more of a concern here than diffusion, the width of the wells has been reduced for this study compared to QRDs designed for diffusive purposes. The losses in the wells caused by the viscous and thermal conduction have been considered. To predict the surface sound absorption, the method used by Mechel is used. The use of a resistive layer on the surface to improve the absorption of the structure is investigated in some detail.

As shall be shown later, a optimum diffuser does not necessary produce the best absorption. It is possible to produce a configuration that is a better absorber than those based on the quadratic residue sequence. This is done by producing many well-tuned and well-distributed resonance frequencies by choosing the depth sequence in one period using an optimization approach.

I. PREDICTION METHOD

Two methods have been used to predict the absorption on the surface of profiled diffusers; one uses the average

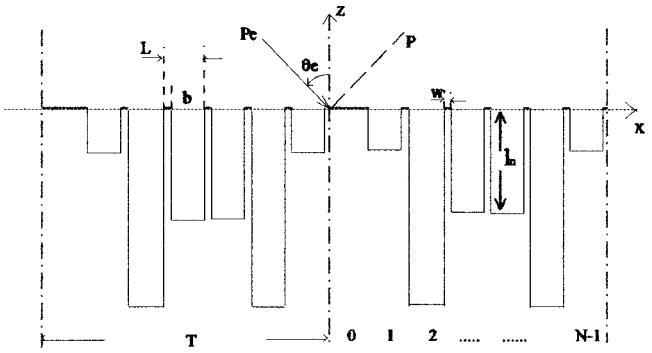

FIG. 1. One-dimensional quadratic residue diffuser for $N=7$, 2 periods shown.

surface admittance, another uses Fourier analysis. The former was introduced by Kuttruff by assuming uniform pressure on the entrance of the structure. In many cases, however, as he indicated, it is only an approximate method, as it does not properly model the mutual interference between the differently tuned wells caused by different depths in one period. The later method, i.e., Fourier analysis, more correctly considers the coupling between the wells, and thus is more rigorous. In this paper only Fourier analysis method will be discussed and used in the predictions. Figure 1 shows a sketch of a one-dimensional QRD structure, together with the coordinate system. The expression of the depth sequence, l_n, in one period of a one-dimensional QRD is well known[1] as

$$l_n=\frac{c \bmod(n^2,N)}{N(2\,f_r)}, \quad n=0,1,...,N-1. \tag{1}$$

where f_r is the design frequency, N is the prime number, and c is the speed of sound in air. As shown in Fig. 1, the diffuser is periodic with N wells in one period. The period is $T=N*L$ wide with the grid length of one well, $L=b+w$, where b is the well width and w is the wall thickness between the wells.

A. Energy losses in the wells

Normally the well width of the QRD is quite large to minimize absorption. However, in this study, the width of the wells needs to be reduced to get higher absorption. In this case, the losses caused by the viscous and thermal conduction in the narrow wells cannot be neglected. In general, in the middle frequency range of interest, the width of the wells b is usually quite narrow compared with the incident wavelength, i.e., $b \ll \lambda/2$, so that there is only fundamental mode propagating in each well.

When describing the sound propagation in a narrow slit, three waves will be of concern: propagating wave, thermal wave, and shear wave. In many cases of practical interest, the attenuation caused by the thermal wave and viscous wave only occurs in the boundary layers, which are of a fraction of a millimeter thick. Usually their effects can be incorporated into the boundary conditions on the propagating wave. Morse and Ingard[9] derived the complex wave number in a cylindrical tube. The method can also be used for a narrow slit.

Assuming that the slit has two infinite parallel rigid walls, then it is somewhat more convenient to run the z axis along the central line of the slit. Because the boundary surface is rigid, the particle velocity u and the temperature fluctuation τ at the surface are zero. The propagation wave for fundamental mode has acoustic pressure p_p, temperature τ_p, and normal u_{px} and tangential u_{pz} velocity:[9,10]

$$\begin{aligned}
p_p&=\cos\left(\frac{\pi q x}{b}\right)e^{-jk_t z}e^{j\omega t},\\
\tau_p&=\frac{\gamma-1}{\alpha\gamma}\cos\left(\frac{\pi q x}{b}\right)e^{-jk_t z}e^{j\omega t},\\
u_{px}&=\frac{1}{j\omega\rho}\,\frac{\pi q}{b}\sin\left(\frac{\pi q|x|}{b}\right)e^{-jk_t z}e^{j\omega t},\\
u_{pz}&=\frac{k_t}{\rho c k}\cos\left(\frac{\pi q x}{b}\right)e^{-jk_t z}e^{j\omega t},
\end{aligned} \tag{2}$$

where $k_t^2=k^2-(\pi q/b)^2$, $k=\omega/c$ is the wave number, ρ is the air density, and $\gamma=(C_P/C_V)$ is the ratio of the specific heat, $\approx 7/5$ for air. The constant q can be adjusted to fit the boundary conditions by incorporating the thermal wave and shear wave in the boundary layers. Following the method used by the Morse and Ingard,[9] for width $b \gg d_v, d_h$, where d_v, d_h are the thickness of the viscous and thermal boundary layers, q can be defined for a narrow slit:

$$(\pi q)^2=-(1-j)k^2 b[d_v+(\gamma-1)d_h]. \tag{3}$$

This gives the propagation number as

$$k_t=\sqrt{k^2-\left(\frac{\pi q}{b}\right)^2}\approx k+\frac{k}{2b}(1-j)[d_v+(\gamma-1)d_h] \tag{4}$$

for air at atmospheric pressure and room temperature, d_v, d_h can be determined[10] as

$$d_v=\sqrt{\frac{2\mu}{\rho\omega}}\approx 0.21\frac{1}{\sqrt{f}}, \quad d_h=\sqrt{\frac{2K}{\rho\omega C_p}}\approx 0.25\frac{1}{\sqrt{f}}\ \text{(cm)}, \tag{5}$$

where f is sound frequency, and μ, K, and C_p are the properties of gas. μ is the coefficient of viscosity, K is the thermal conductivity, and C_p is the heat capacity per unit mass at constant pressure.

Once the sound propagation in the slit is known, the inward impedance on the surface of well with length l_n can be easily derived as

$$Z(l_n)=-j\rho_e c\frac{k}{k_t}\cot(k_t l_n), \tag{6}$$

where ρ_e is the effective density of air in the slit:[11]

$$\rho_e=\rho[1+(1-j)d_v/b] \tag{7}$$

so that the inward normalized specific impedance of the well with length l_n is then

$$\begin{aligned}
\zeta(l_n)&=\frac{Z(l_n)}{\rho c}\\
&=-j\{1+(1-j)[d_v-(\gamma-1)d_h]/2b\}\cot(k_t l_n).
\end{aligned} \tag{8}$$

B. Prediction of absorption by QRD

The analysis below closely follows the method used by Mechel.[7] The sound field in front of the diffuser, shown in Fig. 1, is decomposed into the incident plane wave $p_e(x,z)$ and scattered field $p_s(x,z)$, which is made up of propagating and nonpropagating evanescent waves:

$$p(x,z)=p_e(x,z)+p_s(x,z), \tag{9}$$

$$p_e(x,z)=P_e\cdot e^{j(-xk_x+zk_z)},$$

$$\text{where}\quad k_x=k\sin\theta_e,\quad k_z=k\cos\theta_e, \tag{10}$$

$$p_s(x,z)=\sum_{n=-\infty}^{+\infty}A_n e^{j(-x\beta_n-z\gamma_n)}. \tag{11}$$

Since the QRD is periodic, the scattered field is also periodic in x. Therefore the wave numbers in the x and z directions of the spatial harmonics are (the first from the periodicity, the latter from the wave equation)

$$\beta_n=k_x+n\frac{2\pi}{T};$$

$$\gamma_n^2=k^2-\beta_n^2\Rightarrow\gamma_n=-jk\sqrt{\left(\sin\vartheta_e+n\frac{\lambda}{T}\right)^2-1}, \tag{12}$$

where $\lambda=2\pi/k$ is the wavelength. The corresponding radiating harmonics indices n_s, which can propagate to the far field, are determined from

$$\left(\sin\theta_e+n_s\frac{\lambda}{T}\right)^2\leqslant 1. \tag{13}$$

Considering the outward particle velocity along the positive z direction, the relation of pressure and particle velocity on the surface is $\rho c v_z(x,0)=-G(x)p(x,0)$. This gives

$$\cos\theta_e P_e-\sum_{n=-\infty}^{+\infty}\frac{\gamma_n}{k}A_n e^{-jxn2\pi/T}$$

$$=G(x)\left[P_e+\sum_{n=-\infty}^{\infty}A_n e^{-jxn2\pi/T}\right]. \tag{14}$$

Since $G(x)$ is periodic with a period T, we apply a Fourier analysis:

$$G(x)=\sum_{n=-\infty}^{+\infty}g_n e^{-jn(2\pi/T)x},$$

$$g_n=\frac{1}{T}\int_0^T G(x)e^{+jn(2\pi/T)x}dx. \tag{15}$$

Equation (15) inserted into the boundary condition gives, after multiplication by $e^{jm(2\pi/T)x}$ and integration over T:

$$\sum_{n=-\infty}^{+\infty}A_n\left(g_{m-n}+\delta_{m,n}\left(\frac{\gamma_n}{k}\right)\right)=P_e(\delta_{m,0}\cos\theta_e-g_m);$$

$$m=-\infty,\ldots\ldots,+\infty, \tag{16}$$

where

$$\delta_{m,n}=\begin{cases}1, & m=n\\ 0, & m\neq n,\end{cases}$$

TABLE I. Depth sequences of different structures (in cm).

		Optimization			
		Without mirror-image		With mirror-image[a]	
QRD	Random sequence	1	2	1	2
0.0	0.0	3.6	2.5	10.0	4.8
2.5	1.0	10.0	10.0	9.2	3.4
10.0	3.0	5.6	3.8	8.5	3.7
5.0	5.0	9.1	9.4	7.2	8.6
5.0	7.0	6.7	5.9	5.8	5.7
10.0	9.0	8.2	7.3	3.9	8.3
2.5	10.0	4.5	4.8	4.3	10.0

[a]See Sec. II B.

and the infinite large system of equations will be terminated at the index limits $n,m=\pm 2*N$, where N is the number of wells in one period. By solving the above equations, the coefficients A_n can be obtained.

The absorption coefficient of diffuser is then

$$\alpha(\theta_e)=1-\left|\frac{A_0}{P_e}\right|^2-\frac{1}{\cos\theta_e}\sum_{n_s\neq 0}\left|\frac{A_{n_s}}{P_e}\right|^2\sqrt{1-(\sin\theta_e+n_s\lambda/T)^2}; \tag{17}$$

the summation runs over radiating spatial harmonics only. Evidently the second term is the specular reflection, and the third term is due to scattering.

If a resistive layer is applied on the surface of structure to enhance the absorption, the only replacement made in the above method is $G(x)\rightarrow 1/(R+\zeta_{\text{well}})$, where R is the normalized effective impedance of the resistive layer, and ζ_{well} is the input normalized impedance of a well.

II. EXPERIMENTAL AND THEORETICAL RESULTS

A. Methods of measurement

Two types of samples, one with constant length slits and the other a one-dimensional QRD, were built from a square tube that had a cross-section size 54 mm×54 mm. Because of tube's size, the QRD are limited to: prime number 7, design frequency $fr=980$ Hz, the maximum length of wells 10 cm, well width $b=6$ mm, and separation wall thickness $w=1$ mm. The length sequence has been listed in Table I, as ''QRD.'' The wells were terminated by MDF (Medium Density Fiberboard) which has been varnished three times. The wells are separated by aluminum sheets. In order to compare fairly, the corresponding constant length structure is composed of seven slits with the same width as the QRD and with all the wells having a length of 10 cm. The whole sample is sealed with petroleum jelly as good as possible.

A method similar to the standard two microphone method[12] is used to measure the surface impedance of the sample in the impedance tube. Consequently, the results presented here are restricted to normal incidence. Furthermore, the normal incidence absorption coefficient is computed for the impedance from the well-known formula:[13]

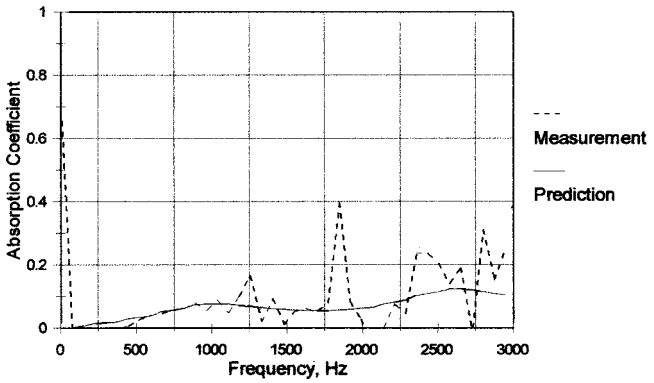

FIG. 2. Absorption coefficient of constant length slit sample.

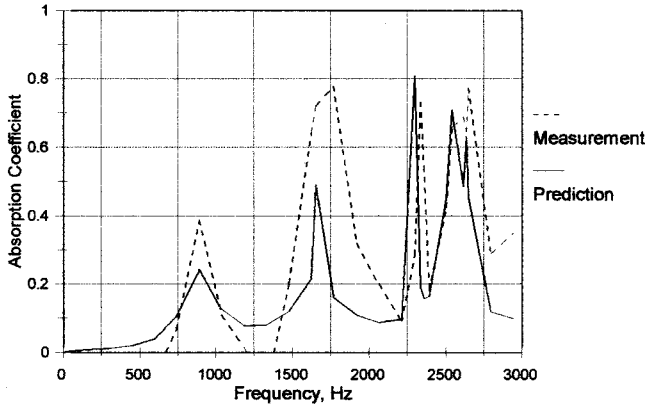

FIG. 3. Comparison between the prediction and experiment for the QRD.

$$\alpha = \frac{4\,\mathrm{Re}(\zeta)}{[1+\mathrm{Re}(\zeta)]^2+[\mathrm{Im}(\zeta)]^2}, \tag{18}$$

where $\mathrm{Re}(\zeta)$ and $\mathrm{Im}(\zeta)$ are the real part and imaginary part of the normalized impedance, respectively.

The effect of the resistive layers is also tested. A thin wire mesh with resistance 550 rayl (MKS), whose normalized specific acoustic impedance is 1.325, is applied in front of the sample.

B. Theoretical prediction

To predict the experimental results, there are a few things that should be noted:

First, because the sample is set up in the impedance tube with rigid walls, the prediction in Sec. I B cannot be used directly. The period must be doubled to take into account the mirror imaging effect of the side walls. For example, considering the tested QRD with $N=7$, the depth sequence in one period is 0 1 4 2 2 4 1. An image sequence 1 4 2 2 4 1 0 will be created by the rigid walls. So, in fact, this system has 14 elements in one period.

Second, when predicting the absorption coefficient of the sample with wire mesh, the mass effect of the wire mesh has to be considered. In most cases, wire mesh can be treated as rigid. But a thin wire mesh is flexible, and there will be an inertial mass contribution resulting from the induced motion of the sheet.[14] So the *normalized effective impedance* of the wire mesh is

$$R = \left[\frac{R_m(\omega m)^2}{R_m^2+(\omega m)^2} + j\,\frac{R_m^2(\omega m)}{R_m^2(\omega m)^2}\right] \Big/ \rho c, \tag{19}$$

where R_m and m are, respectively, the resistance and mass per unit area of wire mesh.

C. Results and discussions

For conciseness, the following abbreviations in the normalized impedance graphs will be adopted throughout this paper. The real part of normalized impedance will be *R*, and the imaginary part I.

Figures 2 and 3 show the predicted and measured sound absorption coefficient for the constant slits and QRD without wire mesh, and Figs. 4 and 5 show the results with wire mesh. The agreement is good, especially for the results with wire mesh. Without wire mesh, the absorptions are small and very difficult to measure, especially for the constant slits in Fig. 2. Figure 3 contains two important features. First, around the second peak, the absorptions are higher than prediction, it may due to both the gaps in the QRD structure and the resonant vibration of the aluminum sheet, which separated the wells; Second, there is a very sharp absorption peak around 2330 Hz. This only appears in the prediction if the mirror imaging of the rigid walls is modeled. It would not appear for a straight periodic QRD. Comparing Figs. 2 and 3, it is clear that the absorption of the QRD is much higher than the corresponding constant slits. In Figs. 4 and 5, it can be seen that the resonant frequencies are slightly shifted down when the wire mesh is added. This is due to the mass effect introduced by the thin flexible wire mesh. Comparing the absorption in Figs. 4 and 5, higher and more uniform absorption is found for the QRD compared with the constant slit surface.

III. ABSORPTION MECHANISM DISCUSSION

Comparing the absorption of the constant length structure in Fig. 2 and the absorption of the QRD in Fig. 3, although less cells of the QRD are resonating at a particular frequency, it generates higher absorption than the constant slits, even at the resonance frequencies of constant slits, where all slits contribute. This is because the variable depths of the wells create a nonuniform surface impedance that scatters the incident sound. The scattering enhances the propa-

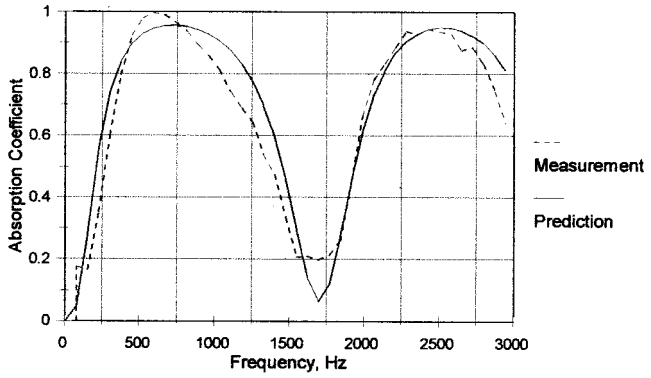

FIG. 4. Absorption coefficient from constant slit sample with 550 Rayls wire mesh on the entrance of the slit.

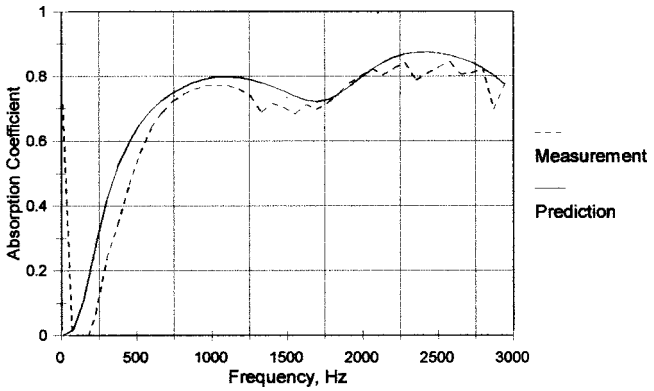

FIG. 5. Comparison between predicted and measured absorption for the QRD with facing wire mesh 550 Rayls.

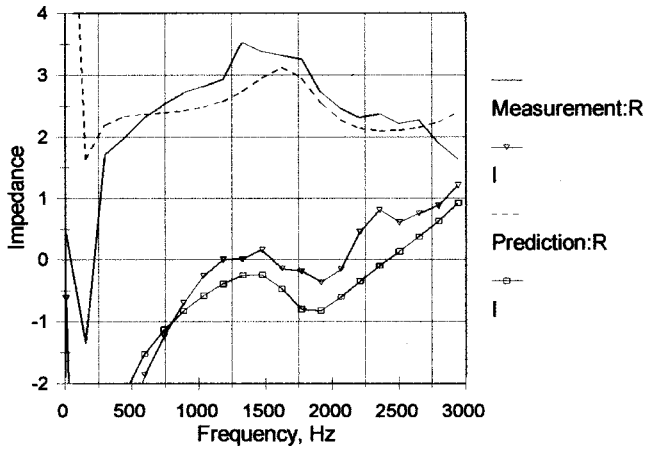

FIG. 7. Normalized specific impedance corresponding to Fig. 5.

gation of the sound wave between wells and hence increases the sound absorption. The impedance graphs of them are typical for pipe systems, except that the QRD has nonuniform resonant frequencies caused by depth variety and slightly higher resistance than constant slits because of the coupling of wells. Applying facing wire-mesh can improve the absorption coefficient significantly across the whole frequency range. Figure 6 shows the normalized specific acoustic impedance corresponding to the constant slits tested in Fig. 4, with a wire mesh glued on the opening of slits, and Fig. 7 shows that corresponding to the QRD tested in Fig. 5 with glued facing wire mesh. For constant length slits, applying wire mesh shifts down the resonance frequencies (the fundamental and first harmonic) because of the mass effect. The real part remains close to the resistance of the wire mesh at 1.325. There is no coupling between the wells that may effect the impedance of whole structure. The absorption is high at the resonance frequencies, but elsewhere is poor. For the QRD, Fig. 7 shows that applying the wire mesh not only shifts down the resonance frequencies, it also smooths the imaginary part and real part of impedance. The imaginary part stays close to zero. This is the reason why high absorption is achieved across the whole frequency range. However, the resistive part is also substantially increased away from unity, leading to a slightly smaller absorption coefficient at resonances. This indicates that the choice of wire mesh is important in optimizing the absorption.

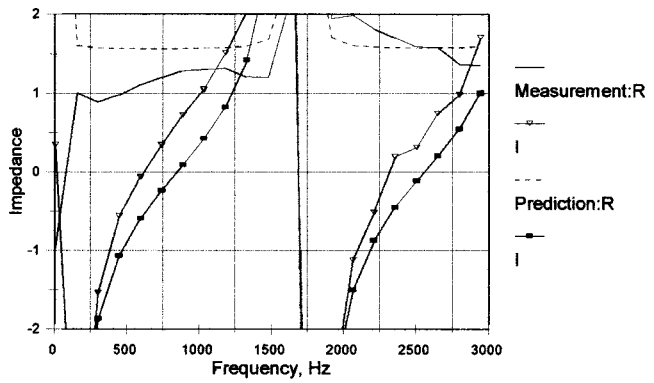

FIG. 6. Normalized specific impedance corresponding to Fig. 4.

IV. OPTIMIZATION

As mentioned before, the depth sequence of a Schroeder diffuser is very important to the absorption of whole structure. In this section, a numerical optimization method,[15] downhill simplex method, is used to tune this sequence. By optimizing the sequence, many well-tuned and well-distributed resonance frequencies can be generated, and higher absorption can be achieved.

A. Optimization process and "absorption parameter" discussion

The process to produce an optimum profiled absorber is based on an iterative process:

(1) An absorber with N wells in one period is constructed with a randomly determined depth sequence.

(2) Absorption coefficients of the absorber is calculated by the Fourier analysis method across the frequency range of interest.

(3) A single figure cost function is calculated which can measure the degree of broadband absorption.

(4) The well depths are altered according to the Downhill Simplex method.

(5) Steps (2)–(4) are repeated until a minimum in the cost function is found indicating an optimum absorber.

There are two cost functions which have been used in the optimization: one is $-\Sigma_{i=1}^{N}\alpha_i/N$, where α_i is absorption coefficient, N is the number of frequencies chosen in the frequency range interested, and the other is $\sqrt{(\Sigma_{i=1}^{N}X_i^2)/N}$, where X_i is the imaginary part of specific acoustic impedance. The first parameter measures the negative of the mean absorption, hence the minimum value gives the highest average absorption. The second one is used because absorption is strongly related to the impedance on the surface of the structure. When the imaginary part of the impedance stays close to zero, high absorption is usually obtained. But one thing that should be noticed here is that the coupling between the wells may cause real part of the impedance to increase and result in less absorption. It is necessary to run the optimization process many times with different starting conditions. The reason for this is that the minimization is being carried out within bounded space. The space hold many local minima within which the minimization routines could be-

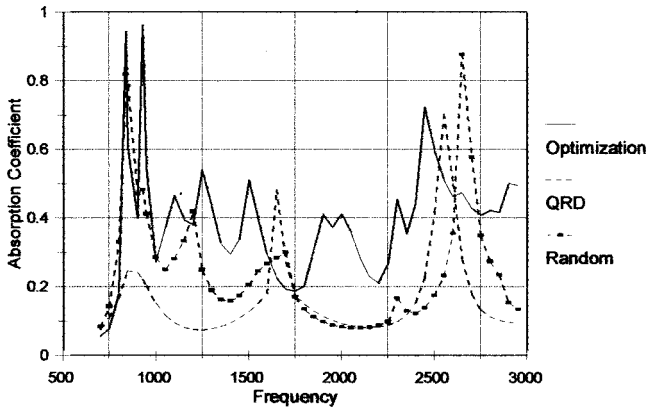

FIG. 8. Comparison of the absorption coefficient for the optimized surface, the QRD, and random sequence structure.

come trapped, particularly at the edges. The results shown below are the best results from many attempts of the iteration process. This does not exclude the possibility that from some particular starting point yet untried there might have a better minimum available.

B. Optimization examples: Theoretical results

As an example, the QRD with the same parameters as that tested in Fig. 3 has been optimized for normal plane wave incidence. In order to compare the results fairly, the maximum lengths of the wells are restricted to 10 cm in the optimization program. The first ''absorption parameter'' cost function, based on the mean absorption coefficient, is used. The frequency range for the optimization is 700 Hz–3000 Hz. The obtained depth sequence of optimized surface structures without and with wire mesh have been listed in Table I as ''Optimization-Without mirror-image'' 1 and 2, respectively.

The results of the comparison with optimized structure, QRD and structure employing random depth sequence, without facing wire mesh on the structure, is illustrated in Fig. 8. The random depth sequence is listed in Table I under ''random sequence.'' It clearly shows that the optimized structure improves the absorption coefficient significantly compared with other two. Its mean absorption coefficient is increased from 0.16 to 0.35 compared with the QRD. In the QRD, the zero depth well does not contribute directly to the absorption as there are no viscous losses due to progragation in this well, so its removal is useful. As there were more nonuniform depths in one period of the optimized structure than the original QRD, more resonance frequencies are generated within the whole frequency range, and the real part of the optimized surface impedance is also improved because of the better coupling of wells when compared to the QRD and random depth sequence. But as shown in Fig. 8, the absorption coefficient is not smooth with many peaks and troughs according to the resonance and anti-resonance frequencies, which is inevitable because of the small resistive part.

The result of the optimization with a facing wire mesh is shown in Fig. 9. This wire mesh has a small flow resistance 55 rayls (MKS), which is a normalized specific impedance of 0.1325. Figure 9(a) shows that the optimized structure is

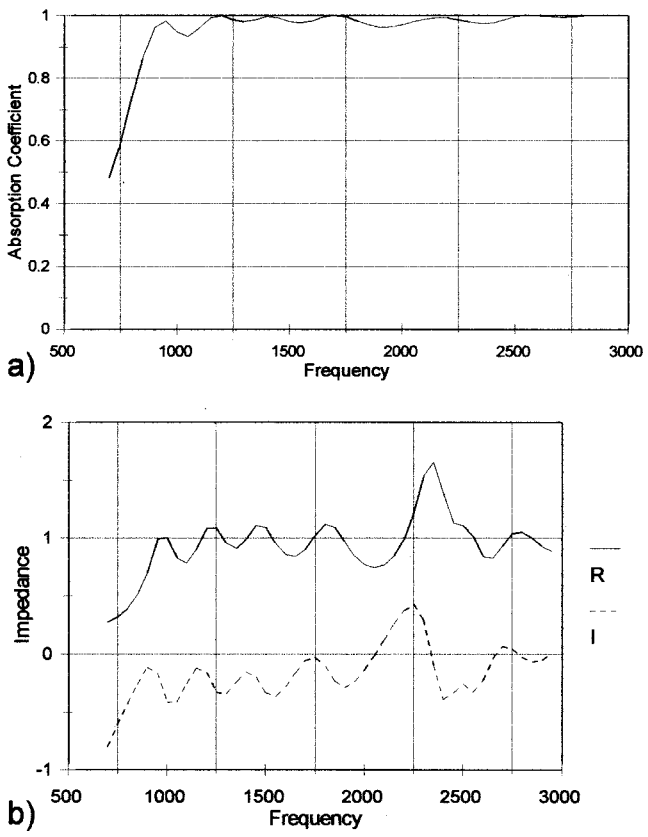

FIG. 9. Optimized structure with facing wire-mesh flow resistance 55 Rayls. (a) absorption coefficient; (b) normalized specific impedance.

obvious a good absorber, with a mean absorption coefficient of 0.96. And Fig. 9(b) shows that, not only does the imaginary part stay close to zero, but the real part of the specific impedance had been raised close to unity. This is more than the flow resistance of the wire mesh can achieve alone. This example demonstrates that optimized the depth sequence can improve the absorption of structure significantly, and downhill simplex method is fast and efficient for this purpose.

As mentioned before, there are two cost functions that can be used to measure the absorption, the following discussion is about the difference in results obtained by using them separately. The base structure is the same as above, but the facing flow resistance is now at 550 rayl (MKS), which is ten times as used before. The results are shown in Fig. 10.

Regarding Fig. 10(a), it is hard to say which cost function is better. The first cost function parameter, average absorption, generated a high absorption across the frequency range; but the second cost function parameter, minimum imaginary Z, produces higher absorption at low frequency. Figure 10(b) also shows other important points. The second, impedance based ''cost function,'' which is intended to produce the imaginary part close to zero, does work. But it also pushes the real part higher at some frequencies at the same time, this induces less absorption at these frequencies; The first, absorption based ''cost function,'' seems to optimize the real part and keep it close to 1, and therefore achieving the higher absorption. Although the imaginary part of impedance is not as close to zero as in the other case, there is no doubt it is optimized as well. Therefore, for the facing sheet

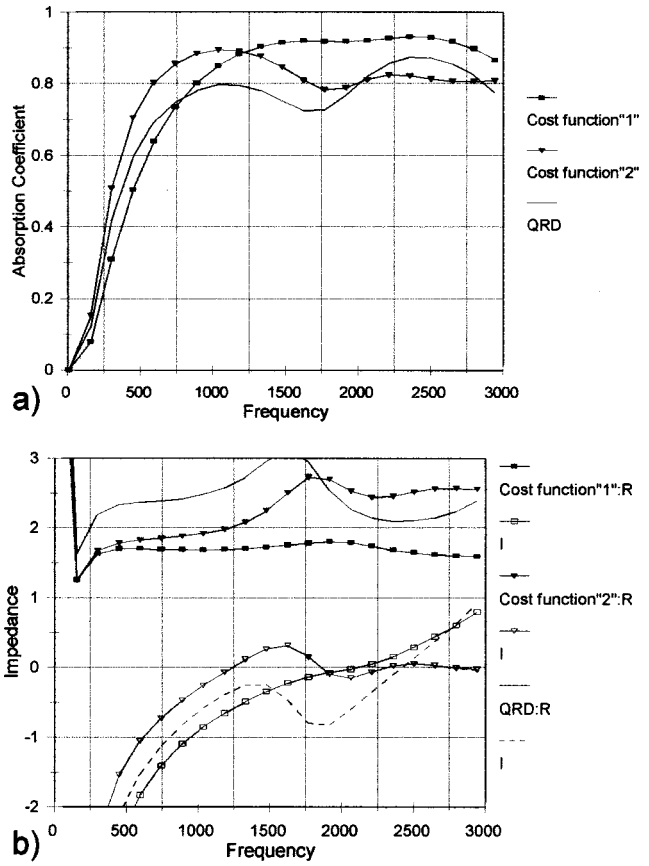

FIG. 10. Comparison of the results using different ''absorption cost functions.'' (a) absorption coefficient; (b) normalized specific impedance.

that has higher resistance, it is better to use the imaginary part cost function in the optimization process, where the real part cannot be reduced. On the other hand, the first cost function is better, for the lower facing resistance.

C. Experimental verification

Again the tests carried out in the impedance tube, and the optimizations had to be repeated with and without wire mesh to take into account of the mirror imaging effect of the impedance tube samples. The resistance of the wire mesh is Rayls (MKS), which is a normalized specific impedance of 0.434. The optimized structures used in the experiments have

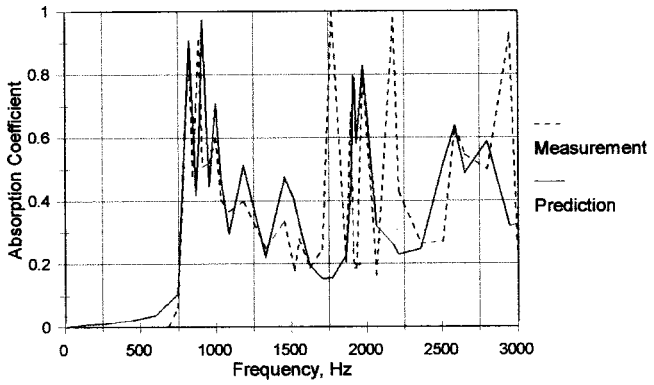

FIG. 11. Comparison of the predicted and measured absorption coefficient for optimized surface.

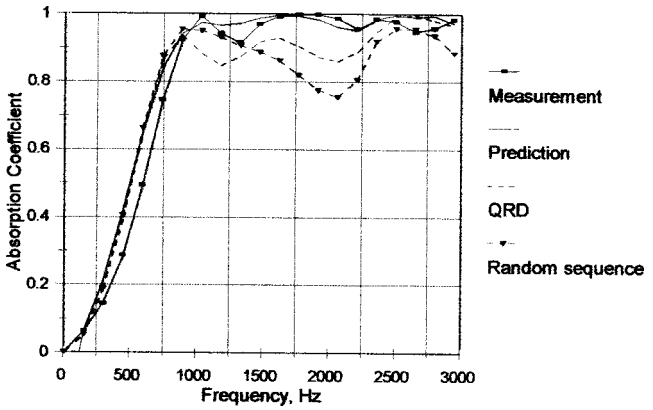

FIG. 12. Comparison between absorption coefficients for predicted and measured optimized surface with wire mesh and predicted the QRD and random sequence structure with wire mesh.

depth sequences shown in Table I, labeled as ''Optimization-with mirror-image'' 1 and 2, where ''1'' represents a depth sequence without wire mesh and ''2'' with wire mesh. The structures are built according to the above depth sequence, and other parameters are the same as tested before: seven wells, $b=6$ mm, $w=1$ mm.

Figure 11 is the comparison between the prediction and experiment absorption data without wire mesh, it shows that in generally they match each other. But there are two peaks which are not expected. It is suggested that they may be caused by the resonant vibration of the aluminum sheets, or higher modes generated in the wells.[16] Figure 12 shows the tested result of the optimized structure with wire mesh; the very good agreement can be clearly seen. The improvement compared with the QRD and random depth sequence structure is also illustrated.

V. CONCLUSIONS

The above study has shown that the variable depth sequence concept can be used to significantly improve the absorption and impedance characteristics of conventional constant depth design. A theory for the prediction of the enhanced absorption was presented and verified by normal incidence measurements on a variety of samples, with and without facing wire meshes. The prediction generally agrees well with experiments and the accuracy is particularly good in cases where a wire mesh is present. An optimization algorithm has been implemented. It was used to demonstrate the improvements in normal incidence absorption performance that can be achieved by optimizing the depth sequence. The optimized structure was tested in impedance tube measurements. The data generally agree with the predicted performance. Further work will be needed to extend the investigation to 2D and to test the optimised samples for the oblique incident sound.

ACKNOWLEDGMENTS

This work was funded by Engineering and Physical Sciences Research Council (EPSRC) of Britain, under Grant No. GR/L34396.

[1] M. R. Schroeder, ''Binaural dissimilarity and optimum ceilings for concert halls: More lateral sound diffusion,'' J. Acoust. Soc. Am. **65**, 958–963 (1979).
[2] P D'Antonio and T. J. Cox, ''Two decades of room diffusers. Part 1: Applications and design,'' J. Audio. Eng. Soc. **46**, 955–976 (1998).
[3] P D'Antonio and T. J. Cox, ''Two decades of room diffusers. Part 2: Measurement, prediction and characterisation,'' J. Audio. Eng. Soc. **46**, 1075–1091 (1998).
[4] K. Fujiwara and T. Miyajima, ''Absorption characteristics of a practically constructed Schroeder diffuser of quadratic-residue type,'' Appl. Acoust. **35**, 149–152 (1992).
[5] K. Fujiwara and T. Miyajima, ''A study of the sound absorption of a quadratic-residue type diffuser,'' Acustica **81**, 370–378 (1995).
[6] H. Kuttruff, ''Sound absorption by pseudostochastic diffusers (Schroeder diffusers),'' Appl. Acoust. **42**, 215–231 (1994).
[7] F. P. Mechel, ''The wide-angle diffuser—A wide-angle absorber?,'' Acustica **81**, 379–401 (1995).
[8] F. P. Mechel, *Schallabsorber* (S. Hirzel Verlag, Stuttgart, 1998), Vol. III, Chap. 5.
[9] P. M. Morse and K. Ingard, *Theoretical Acoustics* (McGraw-Hill, New York, 1968), Chap. 9, pp. 519–522.
[10] P. M. Morse and K. Ingard, *Theoretical Acoustics* (McGraw-Hill, New York, 1968), Chap. 6, pp. 285–291.
[11] J. F. Allard, *Propagation of Sound in Porous Media: Modeling Sound Absorbing Materials* (Elsevier Science, London, 1993), Chap. 4, pp. 48–53 and 59–62.
[12] International Standard, ISO 10534-2, ''Acoustics—Determination of sound absorption coefficient and impedance in impedance tubes.''
[13] H. Kuttruff, *Room Acoustics* (Elsevier Science, London, 1991), third edition, Chap. 2, pp. 30–33.
[14] U. Ingard, *Notes on Sound Absorption Technology* (Noise Control Foundation, Poughkeepsie, New York, 1994), Chap. 1, pp. 1–7.
[15] W. H. Press *et al.*, *Numerical Recipes* (Cambridge University Press, Cambridge, 1989), Chap. 10, pp. 289–293.
[16] F. P. Mechel, *Schallabsorber* (S. Hirzel Verlag, Stuttgart, 1998), Vol. III, Chap. 1.